SAN098-1649C

EFFECTS OF MICROSTRUCTURAL HETEROGENEITY ON BGA RELIABILITY*

SAND--98-1649C

Michael K. Neilsen, Steven N. Burchett, H. Eliot Fang, Paul T. Vianco
Sandia National Laboratories
Albuquerque, New Mexico

CONF-980819--

ABSTRACT

The near eutectic 60Sn-40Pb alloy is the most commonly used solder for electrical interconnections in electronic packages. This alloy has a number of processing advantages (suitable melting point of 183°C and good wetting behavior). However, under conditions of cyclic strain and temperature (thermomechanical fatigue), the microstructure of this alloy undergoes a heterogeneous coarsening and failure process that makes the prediction of solder joint lifetime complex. A viscoplastic constitutive model for solder with an internal state variable that tracks microstructural evolution is currently under development. This constitutive model was implemented into several finite element codes. With this computational capability, the thermomechanical response of solder interconnects, including microstructural evolution, can be predicted. This capability was applied to predict the thermomechanical response of a ball grid array (BGA) solder interconnect. BGAs with both homogeneous and heterogeneous initial microstructures were evaluated. In this paper, the constitutive model used to describe the solder will first be briefly discussed. The results of computational studies to determine the thermomechanical response of BGA solder interconnects will then be presented.

Keywords: BGA, Finite Element Analysis, 60Sn-40Pb Solder, Microstructure

INTRODUCTION

Solder joints were initially designed to be simple electrical interconnections between mechanically interlocked components in electronic packages. As technology advanced, electrical component size decreased, and the number of input/output terminations increased. To accommodate these changes, the number of solder joints per package has increased, while joint dimensions have decreased. The mechanically interlocked components were replaced by plated-through-hole technology which is now being pushed aside by surface mount technology (SMT). With each technological advance, the solder was expected to be not only an electrical conductor but also an increasingly important structural member with smaller and smaller feature size. The benefits of shrinking solder joint dimensions are numerous (e.g., increased speed, greater packing density, etc.) but reliability concerns increase substantially. A key issue of solder joint reliability is joint failure due to thermal cycling since individual components that are soldered together in an electronic package have differing thermal expansion coefficients.

Most current methodologies for evaluating and/or predicting solder joint reliability are empirically based. In these methodologies, specimens are manufactured, tested to failure for given sets of test conditions, and failure models are developed (usually based upon some form of Coffin-Manson relations). These failure models are then applied to similar geometries under different loading conditions to "predict" reliability. There are two major drawbacks to this methodology. First, substantial testing is required for each change such as geometry or material (e.g. lead-free solder) and testing is expensive and time consuming. Second, it is difficult, if not impossible, to assess the effects of critical parameters on reliability through testing alone. To address these drawbacks, validated computational modeling is increasingly being used to assess solder joint response and reliability.

Computational modeling of solder interconnects is exceedingly difficult. To predict the thermal and structural responses of any system, three elements must be defined; the geometry, the loading (including boundary conditions) and the material response (including failure). Solder interconnects present challenges in each of these elements. First, solder interconnects form during processing, therefore the local geometry of the solder interconnects will vary in size and shape, and may have imperfections. Additionally, the size of the solder interconnects are small relative to the package but are numerous. Therefore, obtaining the required resolution within the solder interconnects along with the required package geometry is computationally challenging. Second, the loading that can cause thermomechanical fatigue failure is essentially infinitely variable. Environmental thermal parameters such as temperature cycle range, hold times, and rates of temperature change can all affect solder interconnect

* This work was supported by the United States Department of Energy under Contract DE-AC04-94AL85000. Sandia is a multiprogram laboratory operated by Sandia Corporation, a Lockheed Martin Company, for the United States Department of Energy.

DISCLAIMER

reliability. Internal heating of electronic components can additionally affect reliability. Mechanical loading such as shock and vibration can affect reliability. Third, the material response of solder is exceedingly difficult to model computationally. Solder is a viscoplastic material with material parameters that depend upon the current microstructure. The initial microstructure depends upon processing, and the microstructure evolves during thermomechanical loading. Additionally, even if the stress and strain response of solder can adequately be computed, predicting failure is a challenge.

Our efforts have focused upon the development of a viscoplastic, microstructurally dependent, constitutive model for solder. While this model is still being researched and developed, it shows promise to accurately predict the stress state, the evolution of the stress state with thermomechanical loading, and possibly provide a methodology to estimate the initiation of failure in solder interconnects. In this paper, the constitutive model will be briefly discussed. The constitutive model, in its present state of development, will then be applied to predict the thermomechanical response of a ball grid array (BGA) solder interconnect.

CONSTITUTIVE MODEL

A number of viscoplastic models have been developed for solder[1-5]. Several of these models include the initial grain or phase size as a material constant that does not change during the simulations. The viscoplastic model currently being developed is similar in many respects to the previous models; however, this new model incorporates the grain size (Pb-rich phase size) as an internal state variable which evolves during the simulation. A scalar state variable is used to capture isotropic hardening and recovery and a second order state tensor is used to capture kinematic hardening and recovery. Coarsening is expected to have a significant effect on the state of the material, and a state variable which accounts for the reduction in flow strength with coarsening and follows the Hall-Petch relationship is included in the new model.

The proposed internal state variable model for solder has the following standard constitutive relation

$$\dot{\sigma} = \mathbf{E} : \left(\mathbf{d} - \mathbf{d}^{in}\right) \tag{1}$$

where $\dot{\sigma}$ is the Cauchy stress in the unrotated configuration, $\mathbf{E}$ is the fourth-order, isotropic elasticity tensor, $\mathbf{d}$ is the total deformation rate in the unrotated configuration, and $\mathbf{d}^{in}$ is the inelastic deformation rate in the unrotated configuration[6]. The inelastic deformation rate is given by the following equation

$$\mathbf{d}^{in} = \frac{3}{2}\gamma\mathbf{n} = \frac{3}{2} f \exp\left(\frac{-Q}{R\theta}\right)\left(\frac{\lambda_o}{\lambda}\right)^p \sinh^m\left(\frac{\tau}{\alpha(c+\hat{c})}\right)\mathbf{n} \tag{2}$$

where γ is the magnitude of the inelastic rate, f, p, m and Q are material parameters, R is the gas constant (1.987 cal/mole/K), θ is the absolute temperature, λ is the current grain diameter, λ_o is the initial grain diameter, α is a scalar function of the absolute temperature, and c and $\hat{c}$ are state variables. $\mathbf{n}$ is the normalized stress difference tensor which is given by,

$$\mathbf{n} = \frac{\mathbf{s} - \frac{2}{3}\mathbf{B}}{\tau} \tag{3}$$

where $\mathbf{s}$ is the stress deviator, and $\mathbf{B}$ is the second-order state tensor which accounts for kinematic hardening. τ is a scalar measure of the stress difference magnitude,

$$\tau = \sqrt{\frac{3}{2}\left(\mathbf{s} - \frac{2}{3}\mathbf{B}\right) : \left(\mathbf{s} - \frac{2}{3}\mathbf{B}\right)} \tag{4}$$

Competing hardening and recovery mechanisms are captured by the evolution equations for the internal state variables c and $\mathbf{B}$. Evolution of the scalar state variable c is given by

$$\dot{c} = A_1\gamma - (A_2\gamma + A_3)(c - c_o)^2 \tag{5}$$

where c_o, A_1, A_2, and A_3 are material parameters. Evolution of the second-order state tensor $\mathbf{B}$ is given by

$$\dot{\mathbf{B}} = A_4\mathbf{d}^{in} - (A_5\gamma + A_6)\sqrt{\left(\frac{2}{3}\mathbf{B} : \mathbf{B}\right)}\mathbf{B} \tag{6}$$

where A_4, A_5, and A_6 are material parameters. The reduction in flow strength with grain coarsening is captured by the scalar state variable $\hat{c}$. The state variable $\hat{c}$ is related to the current grain diameter, λ, by

$$\hat{c} = A_7\left(\frac{\lambda_o}{\lambda}\right)^{A_8} \tag{7}$$

where A_7 and A_8 are positive material parameters (A_8 is given a value of 1/2 following the standard Hall-Petch relationship between flow strength and grain size), and λ_o is the initial grain diameter. Note that as the grain diameter, λ, increases, $\hat{c}$ decreases in magnitude which has the effect of reducing the flow strength of the material. Evolution of the grain diameter, λ, is given by the following equation

$$\dot{\lambda} = A_{11}\frac{(v_x + v_o)}{\lambda} \tag{8}$$

where A_{11} is a material parameter, v_x the excess vacancy concentration and v_o the equilibrium vacancy concentration. Finally, the generation of excess vacancies due to inelastic deformation is given by

$$\dot{v}_x = A_9\dot{\gamma} - A_{10}v_x \tag{9}$$

where A_9 and A_{10} are material parameters.

This model was implemented into the finite element codes JAC2D[6], JAC3D[7], and JAS3D[8]. A complete description of the constitutive model development and implementation of the constitutive model into a finite element setting is the topic of a paper currently in preparation.

BGA ANALYSES

The currently implemented three-dimensional, viscoplastic, microstructural-dependent constitutive model for solder was applied to predict the thermomechanical response of a single BGA solder interconnect. The assumed three-dimensional geometry of the BGA interconnect is shown in Figure 1. This geometry can be considered to be a solder interconnect at the outer extremity of the grid array. The substrate was assumed to be an FR-4 material with a coefficient of thermal expansion (CTE) of $17\text{x}10^{-6}$ 1/°C, a Young's modulus of 2.5 $\text{x}10^6$ psi ($1.72\text{x}10^{10}$ N/m^2), and a Poisson's ratio of 0.3. The component was assumed to be an alumina ceramic material with a CTE of $6\text{x}10^{-6}$ 1/°C, a Young's modulus of $41.0\text{x}10^6$ psi ($2.83\text{x}10^{11}$ N/m^2), and a Poisson's ratio of 0.21. The CTE used for the solder was a handbook value of $24.7\text{x}10^{-6}$ 1/°C. In the first analysis, the initial microstructure of the solder was assumed to be uniform. Material parameters for modeling 60Sn-40Pb solder with the viscoplastic solder model are given in Table 1.

The bottom of the FR-4 substrate was not allowed to displace in the y-direction, the left side of the FR-4 substrate was not allowed to displace in the x-direction, and a symmetry boundary condition (no z displacement) was applied to the entire front surface of the model (Figure 1). A uniform time-dependent temperature history was applied. Simultaneously, a time-dependent displacement was applied to the component with magnitude of the applied displacement corresponding to the thermal expansion difference between the ceramic component and FR-4 substrate assuming that the distance from the center of the component to the edge of the BGA interconnect was 0.5 inch (this corresponds to an average shear strain of 4.95%). The applied uniform temperature histories used in these computations are shown in Figure 2 and the applied displacement history is shown in Figure 3.

Table 1: Material Parameters - 60/40 Solder

Property	Value
Shear Modulus (psi)	$1.72\text{x}10^6$
Bulk Modulus (psi)	$8.03\text{x}10^6$
Flow Rate (1/sec)	0.7505
Sinh Exponent - m	10.4
Grain Exponent - p	3.0
Alpha - α	1.0
A_1 (psi)	0.0
A_2 (1/psi)	0.0
A_3 (1/psi-sec)	0.0
A_4 (psi)	$3.26\text{x}10^5$
A_5 (1/psi)	$6.61\text{x}10^{-2}$
A_6 (1/psi-sec)	$4.18\text{x}10^{-6}$
A_7 (psi)	$4.455\text{x}10^3$
A_8	0.5
A_9	$1.0\text{x}10^{-3}$
A_{10} (1/sec)	16.6
A_{11} (in^2/sec)	$5.81\text{x}10^{-5}$
Flow Stress – c_o (psi)	$2.5\text{x}10^3$
Grain Size - λ_o (in)	$35.4\text{x}10^{-6}$
Vacancy Conc. - v_0	$1.0\text{x}10^{-9}$

The response of the solder interconnect was computed for three complete thermomechanical cycles. In Figure 4, the computed shear force (resultant load) is plotted as a function of time. This plot clearly shows the time-dependent creep response at high temperature and essentially elastic response at low temperature. In Figure 5, the computed shear force is plotted as a function of temperature. This plot shows the characteristic hysteresis loops and starts to show the effect of microstructural changes on the response. The solder joint exhibits a reduction in strength as its microstructure coarsens. In Figure 6, contours of the accumulated plastic strain in the solder interconnect at the end of three complete cycles is plotted. This plot indicates that the highest magnitude accumulated plastic strains are at corners of the solder interconnect near the alumina ceramic interface with the peak being at Point A. In Figure 7, contours of the computed microstructural coarsening parameter in the solder interconnect at the end of three complete cycles is plotted. This plot also indicates that the highest magnitude of microstructural coarsening is also at corners of the solder interconnect near the alumina ceramic interface with the peak also being at point A. Experimental observations suggest that these locations are the initiation sites for solder interconnect cracking[9].

The next analysis was identical to the first analysis except the initial grain size was not uniform and was instead given the initial spatial distribution shown in Figure 8. The initial grain size varied from a minimum of $35.4\text{x}10^{-6}$ in.

($0.90x10^{-6}$ m) near the FR-4 substrate and ceramic component to a maximum of $70.8x10^{-6}$ in. ($1.80x10^{-6}$ m) near the center of the BGA. Results from this simulation were remarkably similar to the previous simulation. The shear force history was nearly identical to that shown in Figure 4 for the previous analysis. In Figure 9, contours of the computed grain size in the solder interconnect at the end of three complete cycles is plotted. This plot shows that even though the initial grain size was twice as high in the center of the BGA at the beginning of the simulation, after three cycles the largest grains are near the alumina ceramic interface. Recall that in the previous simulation the coarsening rate was also highest near the ceramic interface and near the corners of the BGA. The grain size at Point A for the first two analyses is plotted as a function of the number of thermomechanical cycles in Figure 10. A comparison of these results shows that solder microstructure at critical Point A will coarsen slightly faster when the initial microstructure is heterogeneous. If we assume that a crack is initiated in the solder joint when the grain size reaches a value of $580.0x10^{-6}$ in. ($14.7x10^{-6}$ m) then these results would predict crack initiation at Point A after 175 cycles for the initially homogeneous microstructure and after 165 cycles for the initially heterogeneous microstructure.

Finally, a series of analyses with homogeneous initial microstructures but with different values for the initial grain size were completed. Results from these analyses were similar to the initial analysis. In all of these analyses, the coarsening rate was highest near the ceramic interface and near the corner of the BGA (Point A in Figure 7). In Figure 11, the computed grain size at Point A is plotted as a function of number of thermomechanical cycles for the various analyses. Figure 11 shows that the analyses with initial grain sizes of $17.7x10^{-6}$ in. ($0.45x10^{-6}$ m), $35.4x10^{-6}$ in. ($0.90x10^{-6}$ m), $70.8x10^{-6}$ in. ($1.80x10^{-6}$ m) generated very similar results, but the results were significantly changed when the initial grain size was increased by a factor of 5 to $177.0x10^{-6}$ in. ($4.50x10^{-6}$ m) and by a factor of 10 to $354.0x10^{-6}$ in. ($8.99x10^{-6}$ m). If we again assume that a crack is initiated in the solder joint when the grain size reaches a value of $580.0x10^{-6}$ in. ($14.7x10^{-6}$ m) then these results would predict crack initiation at Point A after 176, 175, 173, 160 and 111 cycles for the BGAs with initial grain sizes of $17.7x10^{-6}$ in. ($0.45x10^{-6}$ m), $35.4x10^{-6}$ in. ($0.90x10^{-6}$ m), $70.8x10^{-6}$ in. ($1.80x10^{-6}$ m), $177.0x10^{-6}$ in. ($4.50x10^{-6}$ m), and $354.0x10^{-6}$ in. ($8.99x10^{-6}$ m), respectively.

SUMMARY

In this paper, the viscoplastic, microstructurally dependent constitutive model currently being developed was briefly discussed. The model, which was implemented into a 3D finite element code, was applied to predict the thermomechanical response of a ball grid array (BGA) solder interconnect. Results from these simulations show that BGA response is relatively insensitive to factor of 2 variations in the initial microstructure.

While this model is still being researched and developed, the computational capability shows promise to accurately predict the mechanical response of solder, the evolution of the microstructure and mechanical response with thermomechanical loading, and possibly provide a methodology to estimate the initiation of failure in solder interconnects. Additional research will focus on obtaining accurate model parameters, developing criteria for crack initiation and crack growth so that cycles to failure can be predicted, and accelerating the computations.

REFERENCES

[1] Akay, H. U., Y. Tong, N. Paydar, 1992, "Thermal Fatigue Analysis of an SMT Solder Joint Using FEM Approach", J. Microcircuits and Electron. Packaging, vol. 116, pp. 79-88.

[2] Pan, T.-Y, W. L. Winterbottom, 1990, "Thermal Cycling Induced Plastic Deformation in Solder Joints", ASME Winter Annual Meeting, Dallas TX.

[3] Hacke, P., A. F. Sprecher, H. Conrad, 1993, "Computer Simulation of Thermomechanical Fatigue of Solder Joints Including Microstructural Coarsening", ASME J. Electronic Packaging, vol. 115, pp. 153-158.

[4] Busso, E. P., M. Kitano, and T. Kumazawa, 1992, "A Visco-Plastic Constitutive Model for 60/40 Tin-Lead Solder Used in IC Package Joints," J. Engr. Mater. Tech., Vol. 114, July 1992.

[5] Guo, Z., A. F. Sprecher, and H. Conrad, 1992, "Plastic Deformation Kinetics of Eutectic Pb-Sn Solder Joints in Monotonic Loading and Low-Cycle Fatigue," J. Electronic Packaging, Vol. 114, June 1992.

[6] Biffle, J. H. and M. L. Blanford, "JAC2D - A Two-Dimensional Finite Element Computer Program for the Non-Linear Quasi-Static Response of Solids with the Conjugate Gradient Method," SAND93-1891, Sandia National Laboratories, May 1994.

[7] Biffle, J. H., and M. L. Blanford, "JAC3D - A Three-Dimensional Finite Element Computer Program for the Non-Linear Quasi-Static Response of Solids with the Conjugate Gradient Method," SAND87-1305, Sandia National Laboratories, Febr. 1993.

[8] Blanford, M. L., "JAS3D - A Multi-Strategy Iterative Code for Solid Mechanics Analysis - Release 1.3", Sandia National Laboratories, Febr. 1993.

[9] Lau, J. H., and Pao, Y. H., "Solder Joint Reliability of BGA, CSP, Flip Chip, and Fine Pitch SMT Assemblies," McGraw-Hill, New York, 1997.

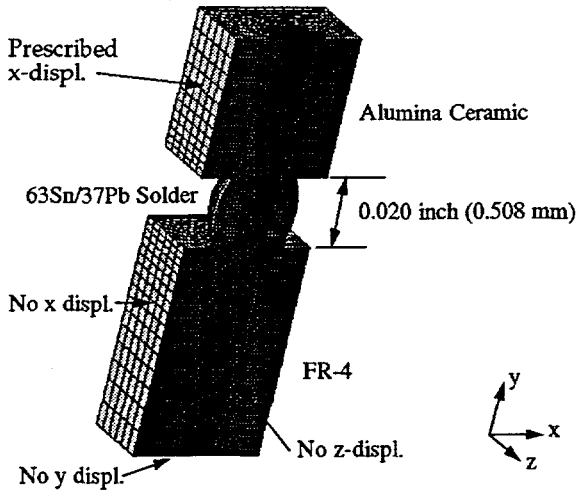

Figure 1: Finite Element Model of Ball Grid Array (BGA) Solder Interconnect.

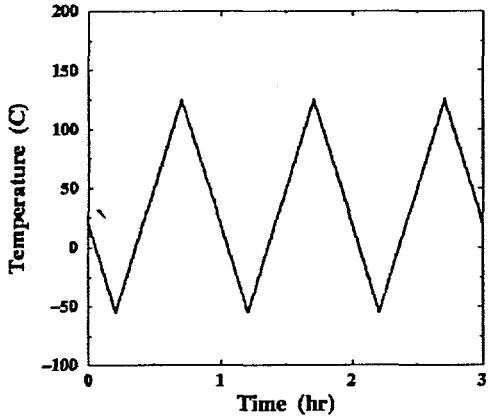

Figure 2: Prescribed Temperature History

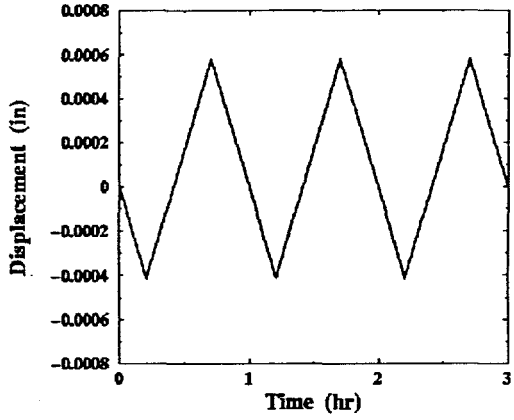

Figure 3: Prescribed Displacement History

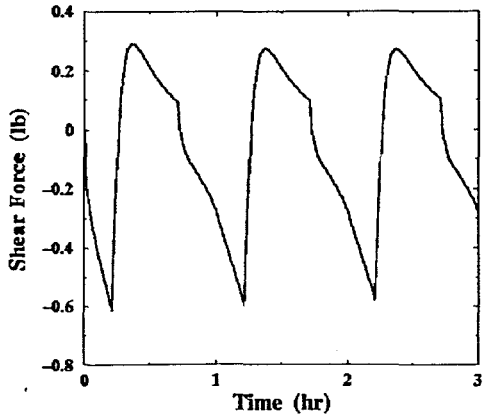

Figure 4: Computed Shear Force vs. Time

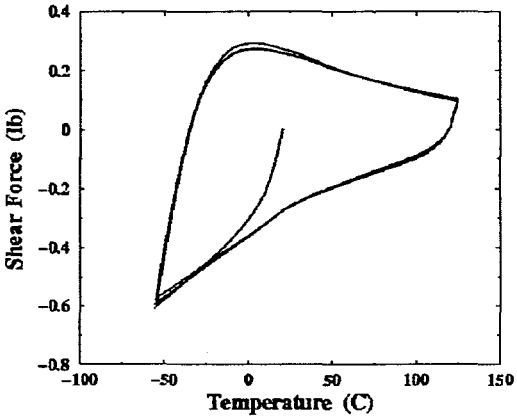

Figure 5: Computed Shear Force vs. Temperature

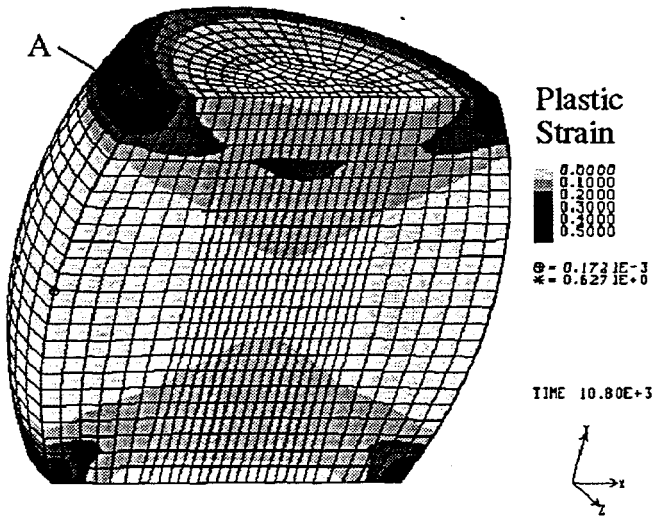

Figure 6: Computed Accumulated Plastic Strain at 3 Cycles.

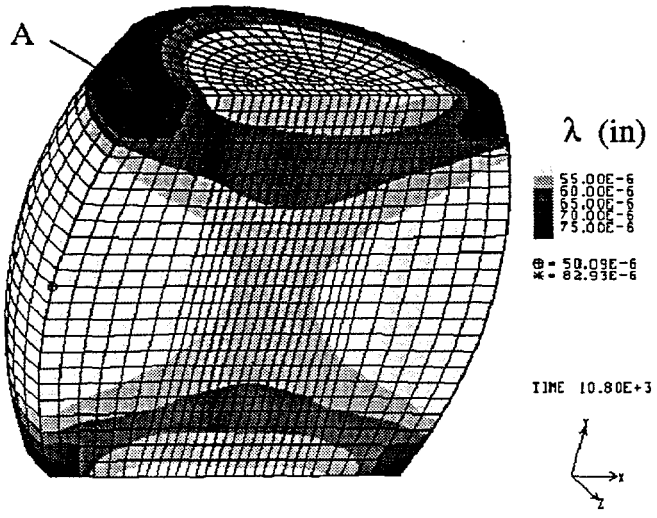

Figure 7: Computed Grain Size at 3 Cycles - Homogeneous Initial Microstructure.

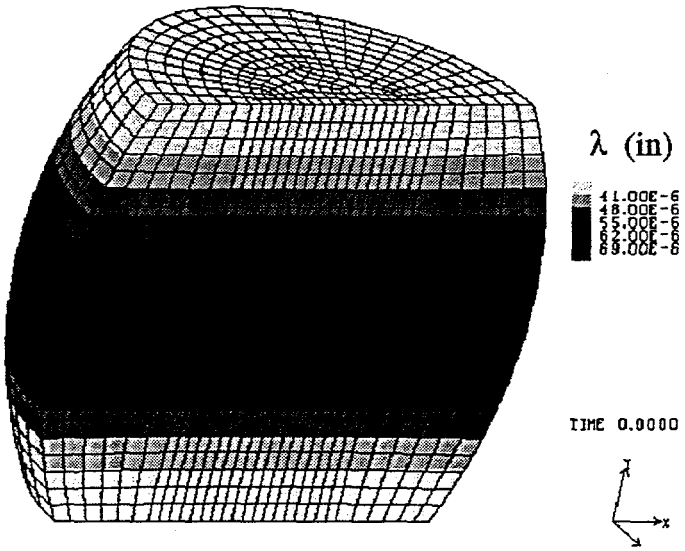

Figure 8: Grain Size Distribution at the Beginning of the Simulation with a Spatially Non-Uniform Initial Distribution.

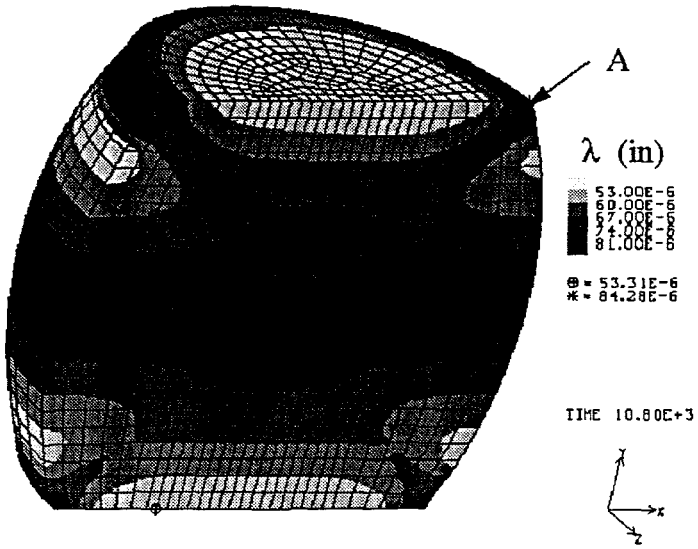

Figure 9: Computed Grain Size at 3 Cycles - Heterogeneous Initial Microstructure.

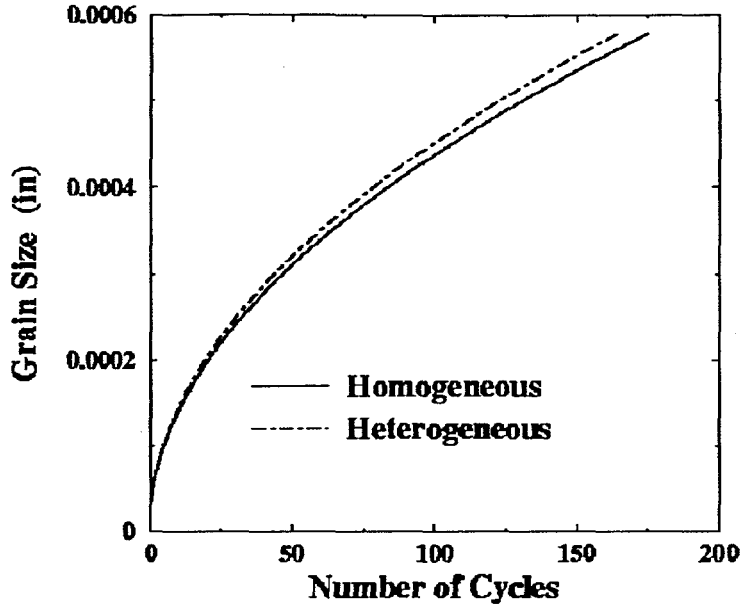

Figure 10: Comparison of Grain Size Evolution for BGAs with Homogeneous vs. Heterogeneous Initial Microstructures.

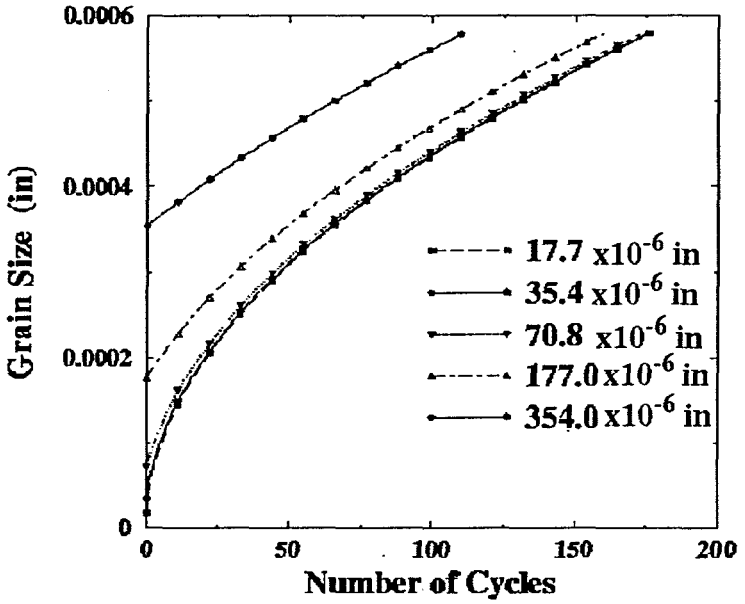

Figure 11: Comparison of Grain Size Evolution for BGAs with Homogeneous Initial Microstructure (Numbers in Legend Indicate Initial Grain Size).